Composite Structures 160 (2017) 435–445

Contents lists available at ScienceDirect

Composite Structures

journal homepage: www.elsevier.com/locate/compstruct

Experimental investigation on structural collapse of a large composite wind turbine blade under combined bending and torsion

Xiao Chen

National Laboratory of Wind Turbine Blade Research & Development Center, Institute of Engineering Thermophysics (IET-Wind), Chinese Academy of Sciences, Beijing 100190, China

ARTICLE INFO

Article history:
Received 18 July 2016
Revised 21 September 2016
Accepted 21 October 2016
Available online 21 October 2016

Keywords:
Local buckling
Delamination
Crushing failure
Debonding
The Brazier effect
Failure mode

ABSTRACT

This study presents a comprehensive investigation on structural collapse of a 47 m composite blade under combined bending and torsion in a full-scale static load test. The primary focus is placed on root causes and failure mechanism of the blade collapse. The investigation consists of three parts. First, video records of the blade collapse are examined on a frame-by-frame basis. Direct evidence is presented on how the blade collapses in progressive chain events. Second, the detailed post-collapse investigation is conducted both in-situ and in laboratory. The critical failure modes and the associated stress/strain state once experienced by the blade are indentified. Third, strain measurements are analyzed to provide quantitative evidence of the process leading to the blade collapse and consequently confirm the findings of this study. It is found that longitudinal compressive crushing failure and the following delamination of the spar cap, which are driven by local buckling, are the root causes of the blade collapse. The constraint of the loading saddle and local reinforcement of the blade section also contributes to the blade collapse. Torsion loads, although exhibiting no significant effect on the blade strength, are found to affect post-collapse characteristics of the blade.

1. Introduction

Wind turbines and their rotor blades continuously increase in size in order to harvest more wind power in higher atmosphere altitude. Structural performance of the blades, which is usually of less concern when the blades are small, becomes more important and it draws considerable attention in recent years [1–7]. As one of the most important structural performance, ultimate strength determines the load-carrying capacity of large blades and it has to be carefully studied. Before a type of rotor blade can be manufactured for mass production, static load tests need to be conducted both before and after fatigue tests according to international test standard IEC 64100-23 [8] to ensure that the ultimate strength of the prototype blade is not reached at a specific load level which represents extreme load conditions. The prototype blade can be certified if no major structural failure occurs when the applied loads reach the load level. These certification tests do not require the blades to be loaded to collapse and they provide not much information on structural response of the blades at their ultimate state, although the information is very valuable and essential for the possible improvement of structural design and/or weight reduction of large composite blades.

Due to the high cost and the potential safety concern associated with the collapse test especially when it is conducted on large blades, there are only a few studies managed to conduct and report their experimental work on the collapse response of composite blades [9–15]. Major attention of these studies has been paid to geometric nonlinearity due to cross-sectional ovalization, or the Brazier effect [9,16], delamination and buckling [10–12] and adhesive joint debonding [13,14]. These studies contributed valuable knowledge to structural response of composite blades. Nevertheless, common agreement has not been fully reached on the root causes because different blades are expected to have different failure mechanisms. Specifically, Jensen et al. [9] concluded that the Brazier effect induced crushing pressure on the blade cross section was the cause of the blade collapse. Overgaard et al. [10] concluded that the blade collapse was caused by geometric nonlinearity in the form of local buckling and delamination instead of the Brazier effect. Chen et al. [11,12] had a similar opinion to Overgaard et al. [10] but emphasized the contribution of the three-dimensional stress to the blade collapse. To make this issue more complex, Yang et al. [13] and Lee and Park [14] concluded that adhesive joint debonding of blade shells was the primary cause responsible for the blade collapse. The studies on full-scale structural collapse tests of large composite wind turbine blades are summarized in Table 1.

E-mail address: drchenxiao@163.com

http://dx.doi.org/10.1016/j.compstruct.2016.10.086
0263-8223/

Nomenclature

SC	spar cap	PS	pressure side
SW	shear web	LS	loading saddle
LP	leading edge panel	SG	strain gauge
AP	aft panel	UD	unidirectional
LE	leading edge		
TE	trailing edge		
SS	suction side		

Table 1
Summary of studies on full-scale structural collapse tests of large composite blades.

Authors	Blade length (m)	Loading condition	Technical approach used	Root causes of failure/failure mechanisms
Jensen et al. [9]	34	Flap-wise bending	Local displacement measurement	Cross-sectional ovalization due to the Brazier effect
Overgaard et al. [10]	25	Flap-wise bending	Strain and local displacement measurement	Local buckling and delamination rather than Brazier effect
Yang et al. [13]	40	Flap-wise bending	Strain measurement	Adhesive joint debonding followed by buckling rather than Brazier effect
Chen et al. [11,12]	52.3	Flap-wise bending	Strain measurement and detailed post-collapse inspection	Local buckling and 3D stress-driven delamination rather than Brazier effect
Lee and Park [14]	48.3	Flap-wise bending	Detailed post-collapse inspection	Adhesive joint debonding followed by torsional failure of the blade section

It can be seen that all blades used in the existing studies were subject to the flap-wise bending, which is the primary loading state of the blades in service. Torsion loads are neglected in the tests because they are usually small compared to the dominant bending loads. Nevertheless, the blades would have lower torsional eigenfrequency as the increase of their size. As a result, the torsional mode may couple with some of the lower bending modes, leading to the concern of structural failure due to combined bending and torsion. According to the author's literature survey, there is by far no experimental work being reported focusing on the ultimate strength and the collapse of large blades under the combined loading state. Although the pioneering work by Berring et al. [17] investigated torsional performance of a 23-m blade under combined bending and torsion, it only focused on the deformation of the blade. In order to find out the potential effect of combined bending and torsion on the blade strength, there is an urgent need of experimental study to be carried out on the full-scale large blades.

Also worth noting is the technical approaches used in the existing studies. Some researchers [9,10,13] primarily worked on quantitative strain and/or local displacement measurements while the others [14] worked on qualitative failure observation from the detailed post-collapse inspection. In the author's opinion, these two approaches have their own advantages in proving useful information on the blade collapse. On the one hand, quantitative measurements provide accurate and precise information on structural response in the entire loading history of the blades. Based on these information it is possible to understand how the blade responses to the applied loads and how different phenomena interact during the loading. On the other hand, the detailed inspection on the post-collapse scene provides direct evidence on failure characteristics of the blades, helping researchers identify the most critical failure modes and indicate the strain/stress state once experienced by the blades. In this regard, it is suggested that two approaches are used together as complements in order to obtain in-depth understanding of the blade collapse.

In view of the aforementioned discussion, this study, aiming to provide new insights into the collapse of large composite blades, conducts a collapse test on a 47-m composite blade under combined bending and torsion. The work is by far, to the author's best knowledge, the first public study reporting the ultimate structural response of the full-scale blades in the combined load state, which represents a more realistic extreme load condition of the blades when their size becomes large. Attempt is made to: (1) find out the potential effect of the combined bending and torsion on the ultimate strength and the collapse response of the blade, (2) identify the critical failure modes responsible for the blade collapse, and (3) clarify the failure mechanism associated with interactive nonlinear phenomena such as local buckling, the Brazier effect, delamination and adhesive joint debonding, which eventually lead to the blade collapse.

To facilitate this endeavor, comprehensive methods are used in this study by integrating information from both qualitative investigation and quantitative measurements. Specifically, video records which capture the drastic collapse process of the blade are analyzed on a frame-by-frame basis. A series of progressive chain events occurred at the collapse instance provide direct phenomenological evidence on how the blade collapses at its ultimate state. The detailed post-collapse investigation is conducted in-situ to identify the critical failure modes associated with the blade collapse. Spar cap (SC) samples at the failure region are cut from the blade and they are further examined in laboratory to find out more evidence which helps reflect the stress/strain state the blade has experienced. Strain measurements in the failure region are analyzed to understand the development of local buckling and the Brazier effect during the loading history and consequently confirm the findings of the study. Based on all the evidence presented in this study, the most likely failure scenario of the blade is reconstructed, and the plausible failure mechanism is also deduced accordingly at the end of this paper.

2. Blade specimen and test method

2.1. General information of the blade

The test article is a 47-meter long composite rotor blade of 2 MW wind turbines. It is made of glass fabrics and vacuum

infused with epoxy resin. The blade has a box-spar construction with two shear webs (SWs) bonded to SCs. Balsa woods are used as core materials in sandwich panels of blade shells up to 30 m from the blade root. PVC foams are used in sandwich panels of blade shells from 30 to 47 m and in two SWs. The blade is pre-bent to 2 m at the tip in order to maintain sufficient blade-tower clearance.

The blade is not painted for the ease of attachment of strain gauges (SGs) and visual inspection on blade failure such as laminate cracks and whitening. Before the blade is tested to collapse, it has been sustained flap-wise fatigue loads of 2 million cycles. In order to identify possible significant damage generated during the fatigue test, both visual inspection and nondestructive testing (NDT) using portable ultrasonic instruments were performed thoroughly on the entire blade. Particular focus was placed on failure modes of skin laminate cracks, SC delamination and adhesive joint debonding. The post-fatigue examination did not find any significant damage in the blade due to fatigue.

2.2. Loading setup

A flap-wise static load is applied to collapse the blade according to the test requirements specified in the latest version of international test standard IEC 64100-23 [8] for rotor blade certification. Four winches are used to apply test loads to the blade through pull points on the loading saddles (LSs), see Fig. 1. The loading setup results in the suction side (SS) and the pressure side (PS) of the blade under compression and tension, respectively. Ten layers of triaxial glass fiber composites by wet layup are applied to the blade to strengthen local regions where LSs are mounted on. Applied loads are recorded by load cells mounted on wire ropes transferring pulling forces from winches to LSs. SGs are deployed on the blade outside surface along the blade span to record local strain response of the blade. Draw-wire displacement transducers are used to record displacement of the blade at four LS locations and the blade tip. Three video cameras are placed in different locations to capture the collapse process of the blade.

The blade is expected to exhibit large deflection in the test, leading to changes in load direction with magnitude. Due to a finite distance between attachment points of winches at test site and on the LSs, load direction angles will change when the blade deforms significantly. The change in angle will result in a change to the load direction relative to the blade axis and the moment arm for calculation of the applied root moment and thereby also the moment at any point between the root and the load application point. The locations of four winches are calculated and pre-adjusted in the test site before the collapse test is carried out so that the loading direction would be perpendicular to the blade axis at the maximum bending.

The loading state of combined bending and torsion is achieved by shifting loading lines intentionally from passing shear centers of blade sections as schematically shown in Fig. 2. Several calculations are performed to determine the initial shifting distance, L, at the loading saddle location. First, the twist angle of the blade cross section is calculated using the torsional stiffness obtained from FOCUS6 [18] and the desired twisting moment at 100% test loads. Second, the shifting distance at the twisted state, L', is calculated by dividing the twisting moment by the pulling force. Finally, the initial shifting distance, L, is calculated based on L' and the twist angle at 100% test loads. As a result of these loading setups, the applied twisting moment at 100% test loads is as close as possible to the desired one in the blade sections of concern as shown in Fig. 3. The combined loading approximates a more realistic extreme load condition that the blade is expected to experience in its service life. It can be seen that the twisting moment is considerably smaller than the bending moment. The maximum moments occur at the blade root and they are 7648 kN m and 137 kN m for bending and twisting, respectively.

The test loads are applied to the blade in a step-wise fashion with a 20% load step until 40% test loads, after which a 10% load step is used until the blade collapses. At each load step, the applied loads are held for a short period of time of approximately 10 s before they are increased to the next load step.

3. Collapse response of the blade

3.1. Pre-collapse behavior of the blade

The blade has sustained the 100% test loads without generating any visual damage or audible cracking sounds, suggesting that the blade has adequate load-carrying capacity and structural integrity with reference to the prescribed limit load state. After that, the applied loads continued to increase intending to collapse the blade. During the process when the blade was loading from 130% to 140% test loads, cracking sounds were detected continuously although the blade did not show any vibration or visual damage in the outside shells. Despite these cracking sounds, the blade survived 140% test loads and sustained the loads for a few seconds. When the applied loads just started to increase towards a higher load level, the blade reached its ultimate strength and collapsed catastrophically.

3.2. Collapse process of the blade

It is of interest to examine the collapse process of the blade to provide direct evidence on its ultimate response. Video records which capture the progressive chain events occurred during the blade collapse facilitate this investigation. The images are captured

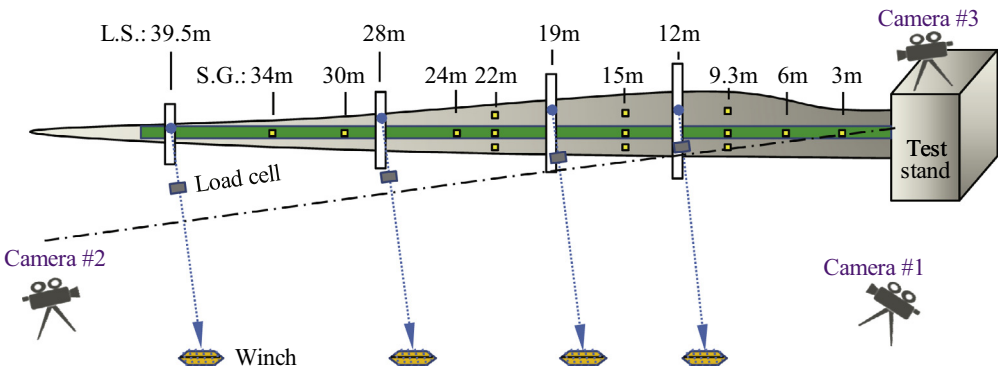

Fig. 1. Loading setup of the blade in the collapse test.

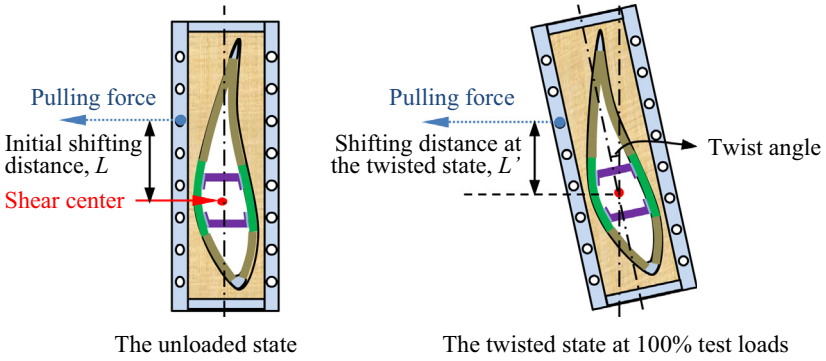

Fig. 2. Introducing combined bending and torsion to the blade.

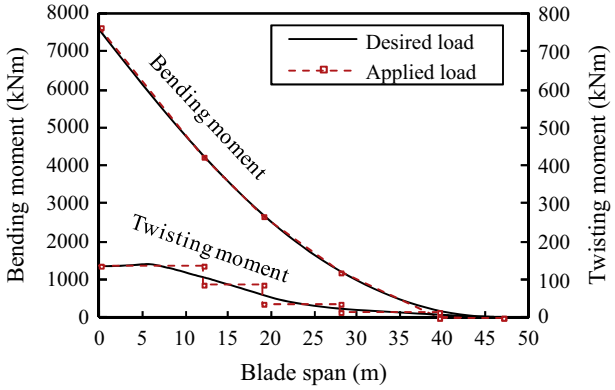

Fig. 3. Bending moment and twisting moment of the blade at 100% test loads.

by a video camera with a record capacity of 30 frames per second and they are examined on a frame-by-frame basis. Typical video frame images are presented in Fig. 4.

Frame #1 captured by camera #1 shows no obvious visual damage in the blade just before the collapse process starts. In Frame #2, longitudinal cracks occur in the intersectional region between SS SC and sandwich panels around the 19-m section where the LS is mounted on. Noting that at this frame, the SS SC exhibits significant local buckling in the form of bulging around the 22-m section. In Frame #3, oblique cracks occur in aft panel (AP) together with the rotation of the LS. The cracks around the 19-m section start to propagate as recoded in the following video frames. In Frame #6, longitudinal cracks are observed near the 28-m section and they further connect to the previous cracks initiated from the 19-m section as shown in Frame #7. The blade collapses in the region from the 15- to 28-m section as shown in Frame #8.

Video records from camera #2 provide clearer images of collapse response of the 22-m section at the beginning of the incident. It is worth noting that significant bulging occurs not only in the SC but also in sandwich panels in the blade cross section as shown in Frame #2. This observation indicates that the entire blade shell, which consists of both SC and sandwich panels, deforms without constraint in the out-of-plane direction at this time instance. Considering that the SC is originally adhesively bonded to the SW, it is impossible for the SC to exhibit large out-of-plane deformation together with the adjacent sandwich panels if the adhesive joints are intact. Therefore, it can be deduced that the significant bulging of the entire blade shell in the SS side is an indication of the failure of adhesive joints in the blade section. Frame #3 shows the same observation of oblique cracks and rotation of the LS as the one captured by camera #1. Furthermore, Frame #4 provides a better view of the fracture of the SS SC and the failure of the blade section near the LS compared with the observation from camera #1. It can be seen that the blade exhibits drastic deformation at this time instance, indicating the loss of the load-carrying capacity of this blade section.

According to the observation presented, several findings can be ascertained. First, a series of progressive chain events occur in the collapse process of the blade. Among them, local buckling of the SS SC in the form of bulging is the phenomenon initiating the collapse process of the blade. Second, debonding of adhesive joints between the SC and the SW accompanies the significant bulging of the blade shell. Third, torsion loads due to the applied twisting moment significantly affect the collapse process of the blade after the occurrence of local buckling.

3.3. Post-collapse characteristics of the blade

Post-collapse characteristics can provide important information on the stress/strain state once experienced by the blade. In this study, the purpose of investigating post-collapse characteristics is to find out evidence which helps identify the critical failure modes associated with the root causes and the possible failure sequence of different failure modes. The investigation is carried out in two levels. The one level is in-situ inspection on the collapsed blade immediately after the test with all evidence 'untouched'. The other level is laboratory examination on samples which are cut from the blade after the in-situ inspection as they are expected to provide further information on the blade collapse.

3.3.1. In situ inspection on the collapsed blade

A close-up of the blade after the collapse test is shown in Fig. 5 (a). It can be seen that the primary failure of the blade ranges approximately from 15 to 28 m from the blade root. The SS SC is separated from AP which exhibits significant fracture near the 19-m section with oblique cracks caused by torsion as previously discussed. Debonding of adhesive joint is observed along trailing edge (TE), leading to the separation of two blade shells. The LS at the 19-m section is dislocated from its original location probably due to the drastic impact load during the blade collapse.

Taking advantage of large openings at various fracture locations, it is possible to examine the interior of the blade. If looking towards the blade tip direction from the blade section around 21 m, one can find that adhesive joints between the SS SC and the SW are completely debonded. Furthermore, the SS SC is delaminated from unidirectional (UD) composites and separated into two portions as shown in Fig. 5(b). If looking towards the blade root direction, one can find that the outside portion of the delaminated SS SC is completely fractured at the 19.9-m section as indicated in Fig. 5(c). The location of fracture correlates well with the one observed in Frame #4 of camera #2. Since the SC is the structural

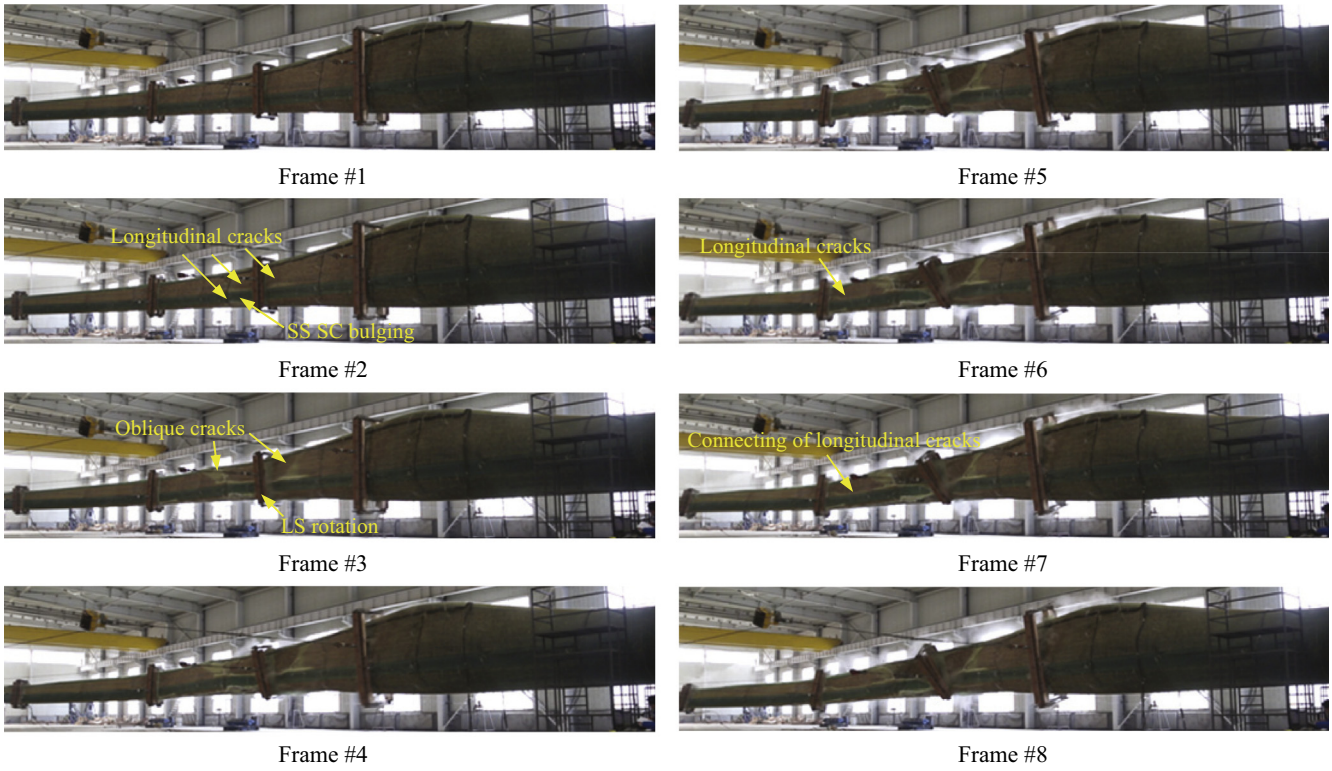

(a) Collapse process captured by camera #1

(b) Collapse process captured by camera #2

Fig. 4. The camera-captured collapse process of the blade.

component primarily responsible for load-carrying, the fracture and the delamination are two critical failure modes which significantly damage the load-carrying capacity of the blade. It should be noted that the PS of the blade was also inspected and there is no failure observed in the SC.

Inspection on SW shows that skin laminates of the leading edge (LE) side SW is fractured with longitudinal cracks at the middle

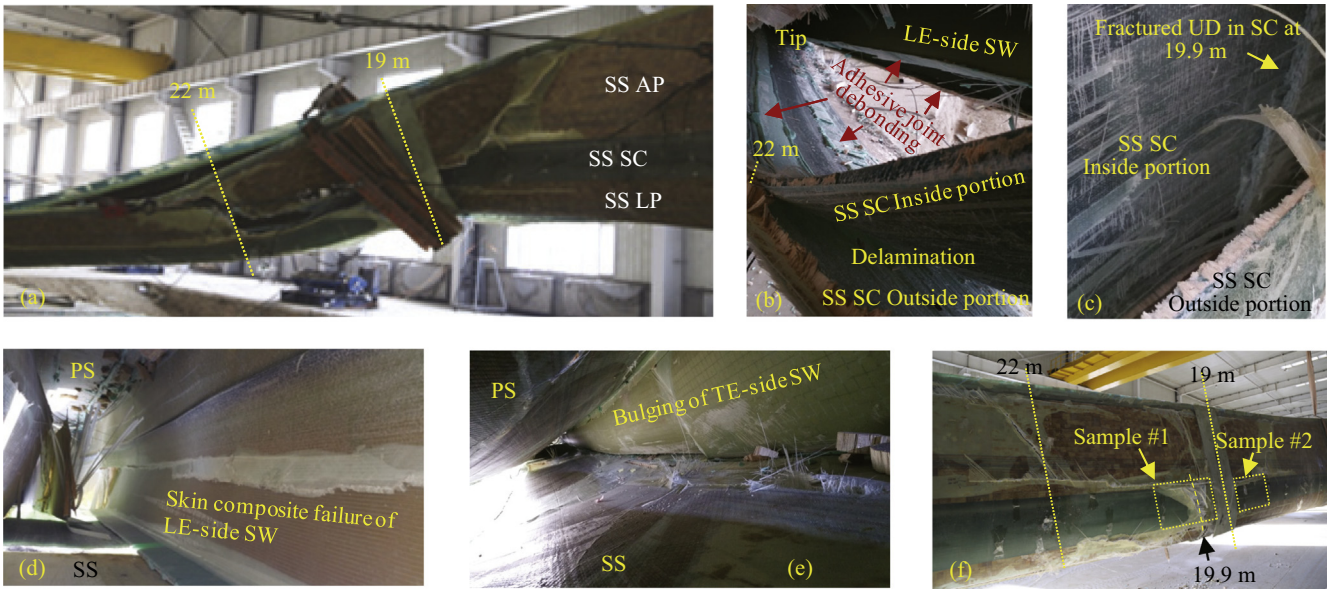

Fig. 5. In situ post-collapse characteristics of the blade.

height of the SW as shown in Fig. 5(d). The TE-side SW is found to undergo significant bulging towards TE with minor cracks in skin laminates as shown in Fig. 5(e). These failure modes in the SW indicate that the cross section of the blade has sustained considerable crushing pressure which imposes transverse compressive forces to the SW. It is deduced that the crushing pressure was caused by the overall flattening, or ovalization, of the blade cross sections, which is also known as the Brazier effect for thin-walled structures under bending. The Brazier effect causes the SC to flatten while the SW inside the blade intends to resists this flattening and is therefore subject to transverse compressive forces, which eventually fail the SW with the failure modes as observed in the blade.

After in-situ inspection, the collapsed blade is replaced to the position as shown in Fig. 5(f). Two SC samples, i.e., #1 and #2, which locate at the failure region are cut from the blade and they are further examined in laboratory to gain more detailed information on the failure of these critical regions.

3.3.2. Laboratory examination on SC samples

SC sample #1, as shown in Fig. 6(a), shows oblique cracks in skin composites. These cracks are regarded to be caused by the tearing force when the blade section is twisted during the blade collapse. Noting that the outside laminates of the sample are transversely cut for the ease of removing to facilitate inspection on the interior. It can be found that multiple delamination exists in the thickness direction of the SC primarily consisted of UD composites, see Fig. 6(b). It is interesting to note that oblique delamination is also found in the middle portion of the SC.

After removing one of the outside laminates, it is found that UD composites of the outside portion of the delaminated SC exhibit significant compressive crushing failure at the fracture location as shown in Fig. 6(c). This failure mode is regarded to be caused by the longitudinal compressive forces sustained by the SS SC. The explosive view of the sample reveals two distinct colors in the delamination surface as shown in Fig. 6(d). The region near the location of UD composite fracture shows a white and bright color while the other region shows a relative dark and green color. This finding implies a possible failure sequence that UD composites at the outside portion of the SS is first subject to longitudinal compressive crushing failure, which initiates delamination at the location of UD composite fracture. After that the delamination further propagates along the SC, creating a dark green color in the delamination surface.

SC sample #2, as shown in Fig. 7, exhibits several interesting failure modes. The first one is delamination of UD composites, which vanishes at the oblique delamination front in the in-plane direction of the SC as indicated in Fig. 7(a). This oblique delamination front is regarded to be caused by the twisting moment as the direction of the delamination front is similar to that of the oblique cracks of AP in this blade section. The second failure mode is the compressive crushing failure of epoxy resin matrix of the outside skin composites characterized by two lines of longitudinal whitening due to transverse compressive forces, see Fig. 7(b). When atten-

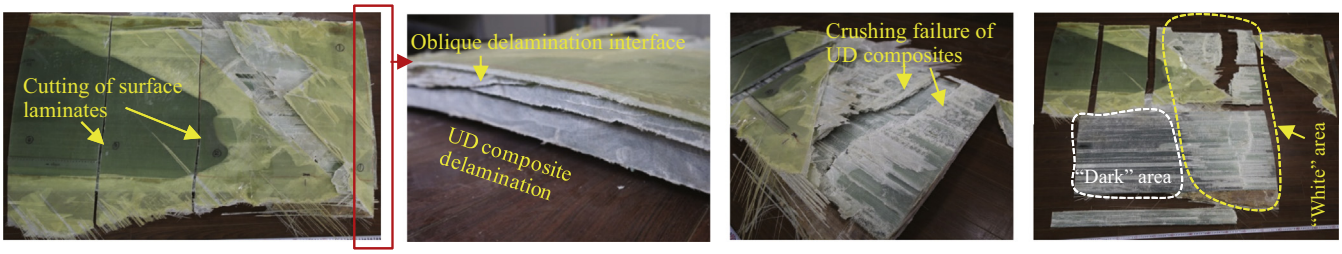

(a) Sample #1 to be examined (b) Delamination (c) Crushing failure (d) Explosive view of the sample

Fig. 6. Laboratory examination on SC sample #1.

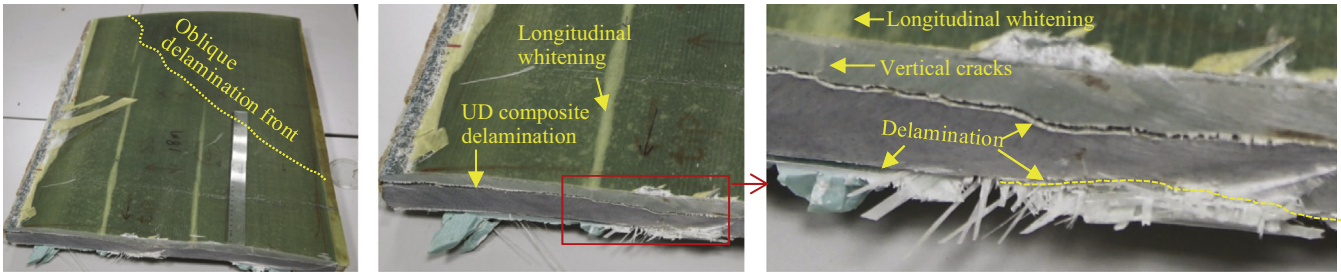

(a) Sample #2 to be examined (b) Delamination and whitening (c) Enlarged image

Fig. 7. Laboratory examination on SC sample #2.

tion is paid to the cross section, it can be found that there are vertical cracks underneath longitudinal whitening lines and they run along the thickness direction of the SC laminates as indicated in Fig. 7(c). The vertical cracks are considered to be caused by transverse tensile forces as they are found to start at the delamination surface of SC and propagate up to the outside skin composites. Moreover, the enlarged image also reveals that delamination does not only occur in the middle but also in the region near the inside surface of the SC as indicated in the figure, implying the existence of transverse tensile stress/strain at the inside surface of the SC.

These failure modes provide important information on the blade collapse. On the one hand, it can be known that the Brazier effect exists in the blade and it is the reason for the longitudinal whitening lines, the underneath vertical cracks and the delamination of the inside portion laminates when the blade cross section is subject to flattening. On the other hand, it can be deduced that three failure modes of UD composite delamination, longitudinal whitening and vertical cracks do not occur simultaneously but in a certain sequence. Considering there is no vertical cracks in the inside portion of the delaminated SC due to the existing delamination surface which stops the further progress of vertical cracks, it can be known that the vertical cracks occur after the UD composite delamination.

From the post-collapse investigation presented, it is clear by far that compressive crushing failure and the following delamination of the SS SC are two critical failure modes directly responsible for the root cause of the blade collapse. Twisting moment applied to the blade is found to considerably affect failure characteristics of the blade by contributing to the oblique cracks in AP and oblique delamination in the through-thickness direction and in the in-plane direction. Furthermore, failure modes observed in the SW and the SC sample #2 suggest the existence of the Brazier effect in the blade. However, it has not been clarified that how these failure modes develop and interact with each other during the loading history leading to the blade collapse. To find out the answers to the question, it is necessary to analyze quantitative strain measurements which record structural response during the entire loading history of the blade and they are presented in the following sections.

4. Local strain response of the blade

Although there are many strain measurements in the blade, the ones deployed in the failure region are of most interest due to the focus of the current study. Local strain response with applied loads measured at the 22-m section is presented as shown in Fig. 8. There are five locations of strain measurements, namely, SC at SS and PS, AP at SS and PS, and LP at PS. The strain measurements of LP at SS are not included in the figure due to inaccurate attachment location of SG. It is noted that straight dash lines are also plotted in the figures to indicate initial slopes of each strain curves.

4.1. Longitudinal strain response

It can be found that all longitudinal strains respond to applied loads in a linear fashion except the one of SC at SS, which exhibits significant nonlinearity starting from 50% test loads as shown in Fig. 8(a). In general, nonlinear behavior of a structure can be categorized into three types from a structural mechanics point of view. The first type is geometric nonlinearity due to large deformation in either global or local structure, the second type is material nonlinearity associated with intrinsic properties of materials used in the structure, and the third type is boundary nonlinearity which involves the change of boundary condition, contact status, etc. For this case, it is not possible for the composite material to undergo nonlinear response due to the low strain level its the longitudinal direction. In addition, there is no detachment between the SG and the blade surface according to post-collapse investigation. It can be concluded that the geometric nonlinearity is the only source contributing to nonlinear strain response of the SC.

Considering that the strain curve is bent towards the positive side with the increase of the applied loads, it can be known that geometric nonlinearity of the SC is developed as local buckling in the form of bulging outward, which leads to the reduction of longitudinal compressive strain of the outside surface of the SC. This finding is important as it provides a strong quantitative evidence to confirm the cause of the SC bulging observed in the video records. It can be known that the development of local buckling of the SS SC during the loading history is a driving factor leading to the bulging of the blade shell and eventually the blade collapse.

4.2. Transverse strain response

When attention is paid to transverse strains of the blade cross section as shown in Fig. 8(b), it is found that transverse strains exhibit nonlinearity. All strain curves bent towards the negative side regardless of the locations of SG. This bent pattern indicates that the outside surface of the blade shell at this cross section is subject to additional transverse compressive strains in addition to its intended transverse strains which are tensile at SS and compressive at PS due to Poisson effect when the blade is primarily under bending. The only explanation to the cause of this bent pattern is the overall flattening of the cross section. This finding provides direct evidence which indicates the existence of the Brazier effect which although has been discussed previously according to post-collapse investigation.

It should be noted that the Brazier effect does not only occur in the 22-m section but also in the 15-m section and the 24-m section. As shown in Fig. 9, two blade cross sections exhibit a bent pattern of transverse strain response similar to that observed in the 22-m section despite difference in the starting load level. Nevertheless, neither SC nor sandwich panels in these two blade sections is found to experience local buckling as all longitudinal strains

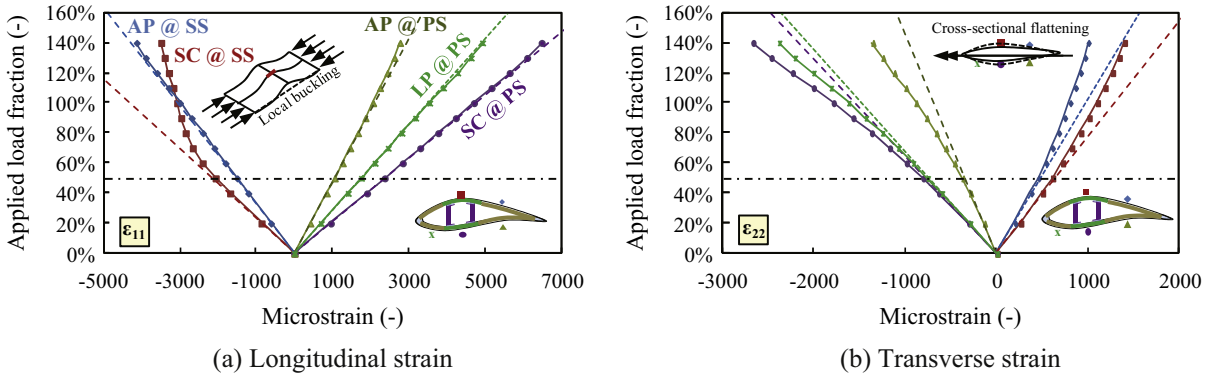

Fig. 8. Longitudinal and transverse strain response of the 22-m section of the blade.

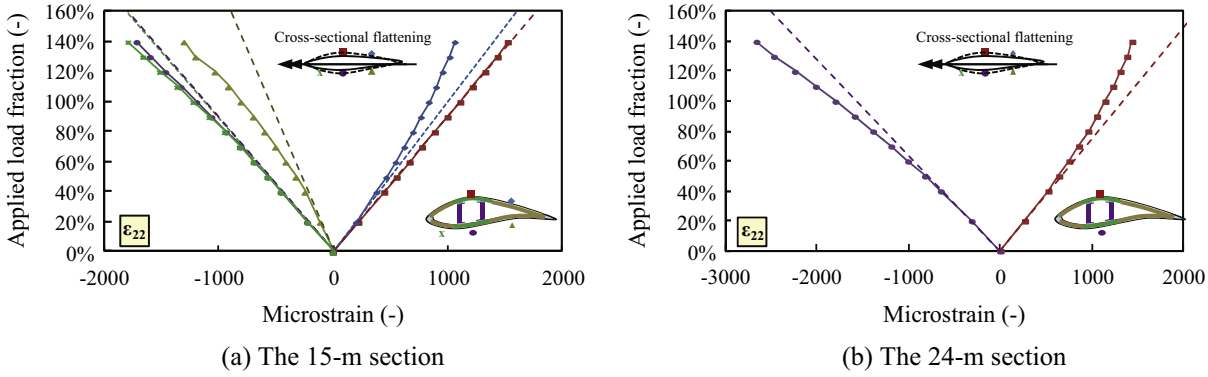

Fig. 9. Transverse strain response of the 15- and 24-m section of the blade.

respond to applied loads in a linear fashion up to the collapse loads.

From the observation on transverse strain response, it is deduced that the overall flattening, or the Brazier effect, of the blade cross sections is not the reason for the blade collapse. Indeed, the cross-sectional flattening is the intrinsic nonlinear geometric behavior of thin-wall structures under bending and this phenomenon can be observed in the blade cross sections which do not fail. According to the investigation on collapse process of the blade using video records, it has been found that the blade collapse is initiated in the cross section around 22 m which is indentified to undergo significant local buckling. It can be therefore concluded that local buckling of the SC is the dominating phenomenon in the loading process leading to the blade collapse.

5. Plausible failure mechanism of the blade

Based on the aforementioned investigation, the root cause and the dominating phenomenon driving the process to the blade collapse are identified. There is, however, one more question to be answered to obtain the whole picture of how the blade collapsed. Considering that the critical failure modes of compressive crushing failure and the following delamination of the SS SC locate at around 20 m while the local buckling of SS SC occurs at 22 m, the relation between these two phenomena needs to be clarified. Unfortunately, there is no strain measurements at the 20-m section to provide direct evidence on how the compressive crushing failure develops during the loading history. Despite the lack of experimental data, a plausible failure mechanism is deduced in this study based on the findings which have been confirmed by the investigation previously presented.

Recall that applied loads are introduced to the blade through LSs, which are built to have enough stiffness to avoid their excessive deformation during the test. Meanwhile, the blade sections at the LS locations are reinforced by wet layups to prevent the blade from local damage. The LS and the local reinforcement are two measures widely used to introduce test loads to the blades. However, they implicitly impose additional constraint to the degree of freedom of the blade cross sections especially in their outward direction. Taking this constraint effect and the previous findings into account, the most likely failure scenario of the load-carrying member, i.e., the SC, can be schematically illustrated in Fig. 10(a), and it is elaborated as follows:

(1) The SS SC is primarily subject to compressive force due to blade bending with the SG attached on the outside surface of the SC at the 22-m section. Two LSs are located at 19-m and 28-m, respectively. The paste line of adhesive joints are applied between SC and SW. Noting that the SW and the PS SC are not plotted in this figure.
(2) The blade as well as the SS SC bend in the flap-wise direction when applied loads are introduced. The outside surface of the SC exhibits larger compressive strain than the inside surface due to its further distance to the neutral axis of bending.
(3) When applied loads increase to 50% test loads, local buckling of the SS SC occurs in the 22-m section in the form of bulging, resulting in additional tensile strain which alleviates compressive strain of the outside surface in this blade section and consequently leads to the bent pattern of the longitudinal strain curve observed in Fig. 8(a). In the meantime, due to the constraint from both the LS and local reinforcement, the SS SC adjacent to the 19-m section is not able to bulge outward following the local buckling of the 22-m sec-

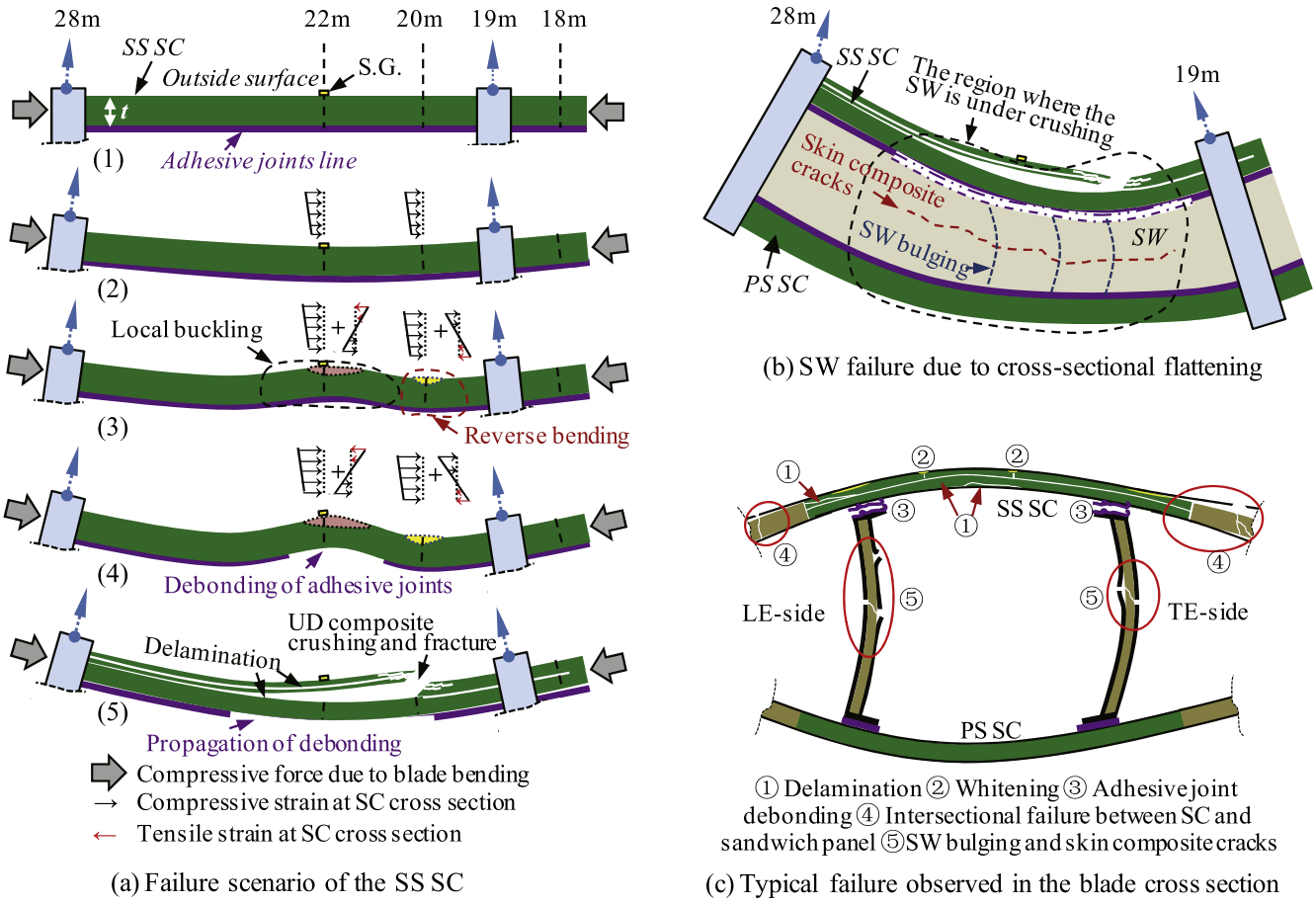

Fig. 10. Illustration of the plausible failure mechanism of the blade collapse.

tion. Therefore, a reverse bending exists in the SS SC from 19 to 22 m. The reverse bending results in additional compressive strain and causes the outside surface of the SS SC to sustain even more compressive strain. Furthermore, the local buckling also leads to the increase of through-thickness tensile stress/strain in adhesive joints which intend to constrain the out-of-plane deformation of the buckled SC.

(4) With the increase of applied loads, the local buckling further develops around the 22-m section and more compressive strains are accumulated in the outsider surface of the SS SC around the blade sections near the LS. Meanwhile, the adhesive joints underneath the buckled SC are not able to sustain large through-thickness tensile stress/strain due to excessive out-of-plane deformation of the SC. The debonding of the adhesive joints releases the constraint imposed to the SC and as a result the entire blade shell, including the SC and the adjacent sandwich panels, around the 22-m section bulges outward drastically. This collapse response is captured by the video image of Frame #2 in Fig. 4.

(5) The significant bulging, or local buckling, of the SC generates considerable compressive strain in the outside surface of the 20-m section. As a result, the laminates experience longitudinal crushing failure due to excessive compressive strain and laminate fracture occurs consequently. The failure of the outside portion of the SC initiates delamination which further propagates along the SC, resulting in the loss of the load-carrying capacity of the blade.

(6) Because the test loads are still applied to the blade, the damaged blade bends and twists drastically due to its loss of the load-carrying capacity as observed in the video image of Frame #3. The bending loads cause the blade cross sections, which at the present have much less stiffness than when they are intact due to the SC failure, to undergo considerable flattening and sustain large transverse crushing pressure induced by the Brazier effect as shown in Fig. 10(b). This leads to post-collapse characteristics of longitudinal cracks and bulging deformation in SW, longitudinal whitening lines and the underneath vertical cracks, and delamination of the inside portion of laminates in the SS SC as previously discussed. The torsion loads, on the other hand, also come into play when the blade loses its strength and cause post-collapse characteristics in the form of oblique cracks in AP and oblique delamination in the through-thickness direction and in the in-plane direction of the SC. Typical failure observed in the blade cross section is schematically shown in Fig. 10(c).

On the basis of all the information presented, it is evident to deduce the plausible failure mechanism of the blade collapse. When the blade is loaded with the offset loading lines, it bends in the flap-wise direction with minor torsion due to the small twisting moment introduced to the blade. The SS of the blade is primarily under compression and experiences local buckling at 22 m starting at 50% test loads. Due to the constraint from the LS and local reinforcement at the 19-m section, the SS SC at 20 m is

not able to deform outward as the one is at 22 m but to exhibit a reverse bending. This leads to considerable increase of longitudinal compressive strain at the outside surface of the SS SC with the development of local buckling. In the meantime, the through-thickness tensile stress/strain increases in the adhesive joints which intend to constrain the local buckling of the SS SC.

At the beginning of the collapse process, the adhesive joints underneath the buckled SC fail. The SS SC and the adjacent sandwich panels around the 22-m section bulge outward significantly. This bulging triggers considerable increase of compressive strains at the 20-m section due to the reverse bending. The outside portion of the SC at the 20-m section fails in the form of longitudinal compressive crushing and the following delamination. In this regard, it is deduced that local buckling of SC, which initiates at 50% test loads, should be considered to be the dominating phenomenon driving the process leading to the blade collapse. The constraint effect from the LS and local reinforcement, on the other hand, is identified to be a significant factor which contributes to the ultimate strength and the failure location of the blade.

Although the overall flattening of the blade cross sections due to the Brazier effect is observed during the loading history of the blade, there is no direct evidence found in this study that it is a likely reason leading to the blade collapse. Nevertheless, the Brazier effect can cause secondary damage to the blade cross sections after the SC failure. Similarly, torsion loads, which are of minor significance when the blade is intact, affect post-collapse characteristics by twisting the failed blade sections. Neither the Brazier effect nor torsion loads is essential for the ultimate strength of the blade as they affect the blade collapse after the critical failure modes of the SC are fully developed.

6. Conclusions and future work

This study presented a comprehensive investigation on a full-scale structural collapse of a large composite blade subject to combined bending and torsion. Video record examination, post-collapse investigation and local strain analysis were conducted to find out both qualitative and quantitative evidence which helps understand how and why the blade collapsed. Major findings of this study include:

(1) The root causes of the blade collapse were indentified to be longitudinal compressive crushing failure and the following delamination of the spar cap at the suction side, which was primarily subject to compressive loads during the test. These two critical failure modes of the spar cap were directly responsible for the loss of the load-carrying capacity of the blade and determined the load level at which the ultimate strength of the blade was reached.
(2) Local buckling of the spar cap in the form of bulging was found to be the dominating phenomenon driving the process to the blade collapse. The loading saddle and local reinforcement contributed to this process by causing a reverse bending in the adjacent spar cap due to their constraint effect, which leads to the increase of compressive strains at the outside portion of the spar cap and the consequent longitudinal crushing failure of the laminates.
(3) This study did not find direct evidence to confirm that the torsion loads had noticeable effect on the ultimate strength of the blade. This is possibly because the magnitude of twisting moment is much smaller than that of bending moment. However, the torsion loads were found to contribute to the post-collapse characteristics once the blade lost its load-carrying capacity due to the spar cap failure.
(4) The strain distribution was found to be not uniform in the through-thickness direction of the spar cap, whose outside portion failed by longitudinal compressive crushing and was further delaminated from the rest portion of the spar cap. This finding emphasizes the importance and necessity of three-dimensional stress/strain analysis for large composite blades with thick laminates.

The structural failure of large composite blade is indeed a complex issue. It involves interactive failure phenomena with multiple sources of nonlinearities. Furthermore, different blades have different design and/or manufacturing techniques, leading to intrinsic difference in structural and material response as a consequence. Although this study tries to provide more understanding to the blade collapse from an experimental perspective, it is very difficult to clarify all the issues without finite element simulations, which are essential to complement the experimental findings. The modeling and simulation of this large blade have been initiated as future work and the relationship between the Brazier effect and local buckling before the blade collapse will be examined in more details.

Acknowledgments

The author of this study would like to acknowledge financial support from the National Natural Science Foundation of China (51405468), the National High-tech Research and Devolvement Program of China (863 Project) (2012AA051303) and the Scientific Research Foundation for the Returned Overseas Chinese Scholars, State Education Ministry, China. The author is very grateful to anonymous reviewers for their comments and suggestions to the original manuscript of this work.

Appendix A. Supplementary data

Supplementary data associated with this article can be found, in the online version, at http://dx.doi.org/10.1016/j.compstruct.2016.10.086.

References

[1] Barnes RH, Morozov EV. Structural optimisation of composite wind turbine blade structures with variations of internal geometry configuration. Compos Struct 2016;152:158–67.
[2] Montesano J, Chu H, Singh CV. Development of a physics-based multi-scale progressive damage model for assessing the durability of wind turbine blades. Compos Struct 2016;141:50–62.
[3] Hosseini-Toudeshky H, Jahanmardi M, Goodarzi MS. Progressive debonding analysis of composite blade root joint of wind turbines under fatigue loading. Compos Struct 2015;120:417–27.
[4] Haselbach PU, Bitsche RD, Branner K. The effect of delaminations on local buckling in wind turbine blades. Renewable Energy 2016;85:295–305.
[5] Eder MA, Bitsche RD, Belloni F. Effects of geometric non-linearity on energy release rates in a realistic wind turbine blade cross section. Compos Struct 2015;132:1075–84.
[6] Chen X, Qin ZW, Yang K, Zhao XL, Xu JZ. Numerical analysis and experimental investigation of wind turbine blades with innovative features: structural response and characteristics. Sci China Technol Sci 2015;58:1–8.
[7] Rosemeier M, Berring P, Branner K. Non-linear ultimate strength and stability limit state analysis of a wind turbine blade, Wind Energy, Online first; 16 June 2015.
[8] International Electrotechnical Commission, "IEC Standard 61400-23, Wind Turbines – Part 23: Full-scale Structural Testing of Rotor Blades", Edition 1.0, 2014-04, IEC; 2014.
[9] Jensen FM, Falzon BG, Ankerson J, Stang H. Structural testing and numerical simulation of a 34 m composite wind turbine blade. Compos Struct 2006;76:52–61.
[10] Overgaard LCT, Lund E, Thomsen OT. Structural collapse of a wind turbine blade – Part A: static test and equivalent single layered models. Compos: Part A 2010;41:257–70.
[11] Chen X, Zhao W, Zhao XL, Xu JZ. Preliminary failure investigation of a 52.3 m glass/epoxy composite wind turbine blade. Eng Fail Anal 2014;44:345–50.

[12] Chen X, Zhao W, Zhao XL, Xu JZ. Failure test and finite element simulation of a large wind turbine composite blade under static loading. Energies 2014;7:2274–97.
[13] Yang JS, Peng CY, Xiao JY, Zeng JC, Xing SL, Jin JT, Deng H. Structural investigation of composite wind turbine blade considering structural collapse in full-scale static tests. Compos Struct 2013;97:15–29.
[14] Lee HG, Park JS. Static test until structural collapse after fatigue testing of a full-scale wind turbine blade. Compos Struct 2016;136:251–7.
[15] Haselbach PU, Branner K. Initiation of trailing edge failure in full-scale wind turbine blade test. Eng Fract Mech 2016;162:136–54. doi: http://dx.doi.org/10.1016/j.engfracmech.2016.04.041.
[16] Brazier LG. On the flexure of thin cylindrical shells and other "thin" sections. Proc R Soc Lond Ser A 1927;213:104–11. doi: http://dx.doi.org/10.1098/rspa.1927.0125.
[17] Berring P, Branner K, Berggreen C, Knudsen HW. Torsional performance of wind turbine blades – Part I: experimental Investigation. In: 16th international conference of composite materials, Kyoto, Japan; July 2007.
[18] Knowledge Centre WMC, FOCUS6 User Guide, July 2015, the Netherlands.